

Dimensional crossover and universal roughness distributions in Barkhausen noise

S.L.A. de Queiroz*

*Instituto de Física, Universidade Federal do Rio de Janeiro,
Caixa Postal 68528, 21941-972 Rio de Janeiro RJ, Brazil*

(Dated: 20th November 2018)

We investigate the dimensional crossover of scaling properties of avalanches (domain-wall jumps) in a single-interface model, used for the description of Barkhausen noise in disordered magnets. By varying the transverse aspect ratio $A = L_y/L_x$ of simulated samples, the system dimensionality changes from two to three. We find that perturbing away from $d = 2$ is a relevant field. The exponent τ characterizing the power-law scaling of avalanche distributions varies between 1.06(1) for $d = 2$ and 1.275(15) for $d = 3$, according to a crossover function $f(x)$, $x \equiv (L_x^{-1})^\phi/A$, with $\phi = 0.95(3)$. We discuss the possible relevance of our results to the interpretation of thin-film measurements of Barkhausen noise. We also study the probability distributions of interface roughness, sampled among successive equilibrium configurations in the Barkhausen noise regime. Attempts to fit our data to the class of universality distributions associated to $1/f^\alpha$ noise give $\alpha \simeq 1 - 1.1$ for $d = 2$ and 3 (provided that suitable boundary conditions are used in the latter case).

PACS numbers: 05.40.-a, 75.60.Ej, 05.65.+b, 75.50.Lk, 75.40.Mg

I. INTRODUCTION

The Barkhausen effect [1] has long been known in magnetism, and reflects the dynamics of domain-wall motion in the central part of the hysteresis cycle in ferromagnetic materials. The intermittent character which is a central feature of Barkhausen “noise” (BN) comes to light already in the original experimental setup. By wrapping a coil around a sample and ramping an external magnetic field at a suitable driving rate, one can detect well-separated voltage pulses across the coil, which are induced by sudden changes of magnetic flux. These in turn result from the microscopic realignment of groups of magnetic moments parallel to the field, i.e. domain-wall motion. For slow driving rates, the integral of the voltage amplitude of a given pulse over time is proportional to the change in sample magnetization, thus giving a measure of the number of spins overturned in that particular event, or “avalanche size”, to recall the terminology frequently used in the study of intermittent phenomena. Modern experimental techniques allow direct observation of domain-wall motion via magneto-optical Kerr effect measurements [2, 3], which demands use of a thin-film sample geometry.

Early proposals for theoretical modelling of BN are reviewed in Refs. 4, 5, whose authors formulate a Langevin description via Fokker-Planck equations. More recently, theoretical interest in the description of the statistical properties of BN has been rekindled, as attempts have been made to establish connections with general theories of non-equilibrium phase transitions and noise phenomena [6, 7, 8, 9, 10, 11, 12, 13, 14, 15, 16, 17, 18, 19]. Here, we shall be concerned with two such connections. The first, motivated by the thin-film results just

alluded to, is the crossover between universality classes [these latter to be properly defined in the context] as one varies the spatial dimensionality of samples; secondly, we extend recently-developed concepts of universality of distribution functions for $1/f^\alpha$ noise [20, 21, 22, 23] to the scaling properties of domain-wall roughness in BN.

Experimentally, double-logarithmic plots of frequency of avalanche occurrence, $P(s)$, against size s turn out to produce unequivocally straight sections, $P(s) \sim s^{-\tau}$, often spanning 3-4 orders of magnitude, before dropping to zero for larger sizes [6, 24]. Such power-law distribution of events has been associated to the concepts of self-organized criticality [6, 7, 25, 26], although other researchers argue that this in fact reflects proximity to a standard second-order critical point, together with an unusually broad critical region in parameter space [8, 12]. Whatever the interpretation, a power-law decay shows up in assorted models used for numerical simulation of BN, both those based on the motion of a single interface in a disordered medium [4, 7, 9, 10] and those which adopt a picture of nucleation of multiple domains in a random-field Ising system [8].

Analogy with the well-established scaling theory of equilibrium phase transitions suggests that, in this case of a non-equilibrium phenomenon, the search for distinct universality classes may lead to a better understanding of the basic mechanisms involved. In Ref. 18, experimental measurements of the exponent τ of avalanche distributions for several soft ferromagnetic materials were found to separate into two distinct groups, namely $\tau = 1.50 \pm 0.05$ (polycrystalline Fe-Si and partially crystallized amorphous alloys) and $\tau = 1.27 \pm 0.03$ (amorphous alloys under stress). It was then proposed that BN for each group of materials listed above belongs to a different universality class of non-equilibrium phase transitions. While the value of τ is a fairly plausible indicator of universality, or lack thereof, between different systems, many questions (prompted again by analogy with static

*Electronic address: sldq@if.ufrj.br

critical phenomena) still remain, such as to how many independent exponents there are, and, of particular interest here, what is the effect of space dimensionality.

Although sample shapes in Ref. 18 were ribbon-like (30 cm \times 0.5 cm \times 60 μ m, to quote typical dimensions), this is far beyond the thin-film regime, for which thicknesses are of the order 5 – 100 nm [2, 3]. Thus the behavior reported in Ref. 18 is expected to be characteristic of fully three-dimensional objects. However, when considering ever thinner samples as in Refs. 2, 3, dimensional crossover effects cannot be ruled out from the outset.

In this work we use a single-interface model, originally introduced in Ref. 7 for the description of BN. We recall (though a detailed discussion will be deferred to Section V) that, for a fixed space dimensionality $d = 2$ or 3, numerical values of e.g. the exponent τ have been found to differ between nucleation and single-interface models (or even between distinct formulations of the latter). Here we work under the assumption that the general features of dimensional crossover to be uncovered are model-independent, similarly to the presence of power-law avalanche distributions. The same assumption is expected to hold as regards the roughness distributions to be investigated in Section IV.

II. MODEL AND CALCULATIONAL METHOD

Here we shall use the single-interface model introduced in Ref. 7. We restrict ourselves to the adiabatic limit of a very slow driving rate, meaning that avalanches are regarded as instantaneous (occurring at a fixed value of the external field). Many experimental setups can be properly described in this approximation [3, 7, 10, 16, 18].

Simulations are performed on an $L_x \times L_y \times \infty$ geometry, with the interface motion set along the infinite direction. The interface at time t is described by its height $h_i \equiv h(x, y, t)$, where (x, y) is the projection of site i over the cross-section. No overhangs are allowed, so $h(x, y, t)$ is single-valued. Each element i of the interface experiences a force of the form:

$$f_i = u(x, y, h_i) + k \left[\sum_j h_{\ell_j(i)} - h_i \right] + H_e, \quad (1)$$

where

$$H_e = H - \eta M. \quad (2)$$

The first term on the RHS of (1) represents the pinning force, u , and brings quenched disorder into the model by being chosen randomly, for each lattice site $r_i \equiv (x, y, h_i)$, from a Gaussian distribution of zero mean and standard deviation R . Large negative values of u lead to local elements where the interface will tend to be pinned, as described in the simulation procedure below. The second term corresponds to a cooperative interaction among interface elements, assumed here to be of elastic (surface

tension) type. In this term, $\ell_j(i)$ is the position of the j -th nearest neighbor of site i . The tendency of this term is to minimize height differences among interface sites: higher (lower) interface elements experience a negative (positive) force from their neighboring elements. The force constant k gives the intensity of the elastic coupling, and is taken here as the unit for f . We assume the boundary conditions to be periodic along x and free along y , so sites at $y = 0$ and $y = L_y$ represent the film's free surfaces and have only three neighbors on the xy plane (except in the monolayer case $L_y = 1$ which is the two-dimensional limit, where all interface sites have two neighbors). The last term is the effective driving force, resulting from the applied uniform external field H and a demagnetizing field which is taken to be proportional to $M = (1/L_x L_y) \sum_{i=1}^{L_x L_y} h_i$, the magnetization (per site) of the previously flipped spins for a lattice of transverse area $L_x L_y$. For actual magnetic samples, the demagnetizing field is not necessarily uniform along the sample, as implied in the above expression; even when it is (e.g. for a uniformly magnetized ellipsoid), η would depend on the system's aspect ratio. Therefore, our approach amounts to a simplification, which is nevertheless expected to capture the essential aspects of the problem. See Ref. 16 for a detailed discussion. Here we use $R = 5.0$, $k = 1$, $\eta = 0.05$, values for which fairly broad distributions of avalanche sizes and roughness are obtained.

We start the simulation with a flat wall. All spins above it are unflipped. The applied field H is set close to the saturation value of the effective field H_e , in order to minimize transient effects. The force f_i is then calculated for each unflipped site along the interface, and each spin at a site with $f_i \geq 0$ flips, causing the interface to move up one step. The magnetization is updated, and this process continues, with as many sweeps of the whole lattice as necessary, until $f_i < 0$ for all sites, when the interface comes to a halt. The external field is then increased by the minimum amount needed to bring the most weakly pinned element to motion. The avalanche size corresponds to the number of spins flipped between two interface stops.

III. SCALING OF AVALANCHE DISTRIBUTIONS AND DIMENSIONAL CROSSOVER

We have collected avalanche histograms for varying L_x , L_y , in a such a way that the number of interface sites $L_x L_y$ varies between 800 and 80,000. The aspect ratio $A \equiv L_y/L_x$ was varied between essentially zero ($d = 2$, one-dimensional interface) and unity ($d = 3$, square interface). For each L_x , L_y we generated 10^5 avalanches. Although it may take $10^2 - 10^3$ avalanches for a steady-state regime to be reached (as measured by the stabilization of H_e against external field H , apart from small fluctuations), we have checked that the only distortion introduced by the transient on avalanche *size* statistics

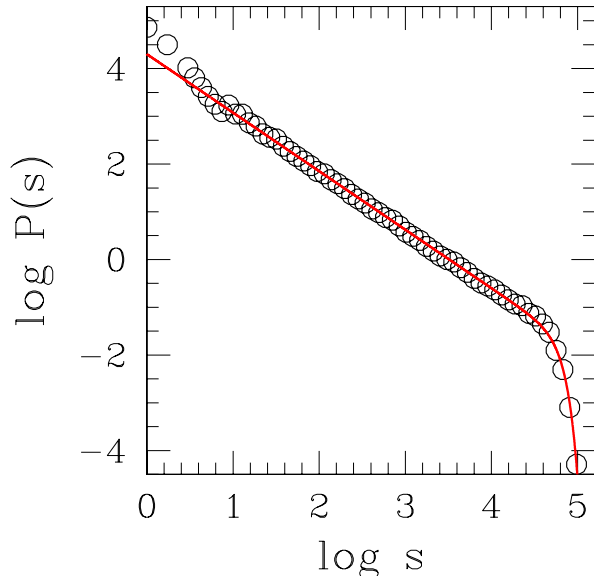


Figure 1: Double-logarithmic plot of avalanche size distribution for $L_x = 60$, $L_y = 30$ (circles). Full line is a fit to the form Eq. (4), for which the optimal parameters are: $\tau = 1.226(6)$, $\delta = 3.6(1)$, $s_0 = 5.97(5) \times 10^4$.

is the one large event occurring at the very start, i.e. on departure from the initial, flat-interface, configuration. We cannot guarantee this to be so when *roughness* is the quantity under investigation, thus data in Section IV have been collected only under steady-state conditions.

The probability distribution $P(s)$ for avalanche size s is expected to behave as

$$P(s) = s^{-\tau} f\left(\frac{s}{s_0}\right), \quad (3)$$

where s_0 is a cutoff related (in experiment) to domain size and/or demagnetization effects [10, 18], and (in simulations) to finite-lattice effects [7, 10], or proximity to a critical point [8]. The specific shape of the function $f(x)$ has been debated. While a simple exponential has often been used, either phenomenologically [7, 8, 10, 24] or (in some special cases) backed by theoretical arguments [5], Gaussian fits, $f(x) \sim \exp(-s^2/s_0^2)$ [17], have been proposed as well. Going one step further, and at the same time trying to keep the number of fitted parameters to a minimum, here we shall follow Refs 27, 28 and fit our data to a *stretched* exponential:

$$P(s) = A_0 s^{-\tau} e^{-(s/s_0)^\delta}. \quad (4)$$

Apart from the overall normalization factor A_0 , one then has three free quantities to fit, which has proved enough for our purposes. A typical example is displayed in Fig. 1. For the roughly sixty $\{L_x, L_y\}$ sets investigated here, the fitted value of δ usually falls in the interval 2.4–3.5, with

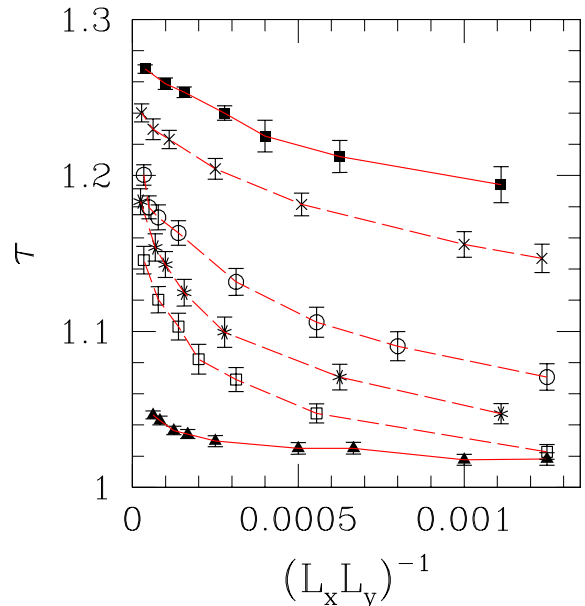


Figure 2: Effective exponent τ from fits of simulation data to Eq. (4), against inverse cross-sectional interface area $(L_x L_y)^{-1}$. Bottom (full triangles linked by full line): monolayer, $L_y = 1$. Top (Full squares linked by full line): $d = 3$, $L_x = L_y$. Intermediate curves (open symbols connected by dashed lines): from bottom to top, aspect ratio $A = 0.005, 0.01, 0.02, 0.1$.

half a dozen cases slightly above that. This is broadly in line with $\delta = 2.32(6)$ quoted in Ref. 27. Though one might argue that a universal value should hold for this exponent, we feel that our results are not accurate enough either to prove or disprove such hypothesis.

On the other hand, the exponent τ which is of central interest here displays systematic variations both against lattice dimensions and aspect ratio. These are displayed in Fig. 2. The overall picture strongly suggests a systematic crossover towards three-dimensional behavior for any fixed (finite) aspect ratio. In addition to this, finite-lattice effects are present as well.

In order to gain a quantitative understanding of this, we recall general ideas of finite-size [29, 30] and crossover scaling [31, 32]. Crossover phenomena reflect the competition between different types of (pseudo-)critical behavior in the vicinity of a multicritical point, at which several characteristic lengths diverge (i.e. their associated fields approach their respective critical values). See e.g. Section VII.A of Ref. 31 for an illustration of the well-known case of thermal-geometric crossover in dilute magnets near the percolation point. Closer analogy with the present case is found in the discussion of dimensional crossover in “layer” magnets [31, 33] (see figure 42 in Ref. 31). Finite-size scaling can be seen as a particular instance of crossover, in which the system’s inverse finite size L^{-1} is an additional relevant field, driving it

away from the true criticality which occurs only in the thermodynamic limit [29, 30, 32]. We now turn to the simulational results exhibited in Fig. 2. Upon increasing sample size, finite-size effects are reduced and the trends followed by the respective exponent estimates differ, depending on whether (i) the aspect ratio A is kept fixed, no matter how small its value (all curves except the lower one), or (ii) $L_y = 1$ is fixed instead (monolayer, lower curve). The latter corresponds to ever-decreasing A as L_x increases, and in the $L_x \rightarrow \infty$ limit is expected to reflect true two-dimensional behavior. Considering, for instance, the curve for $A = 0.005$, for L_x not very large one has exponent estimates closely resembling those of a monolayer with a similar cross-sectional “area”. However, the trend shown implies that this is in fact an apparent behavior, which arises only as long as finite-size effects (represented by L_x^{-1}) are more important than the system’s three-dimensional character (represented by a non-zero value of A). Increasing L_x while keeping A constant, the relative importance of these quantities is eventually reversed, and one crosses over to three-dimensional behavior. These remarks are translated into quantitative statements, as follows. Since the inverse finite size L_x^{-1} and the interface aspect ratio A are both relevant fields, which drive the system away from true two-dimensional behavior, a plausible *ansatz* for the crossover variable is $x = (L_x^{-1})^\phi/A$, where ϕ is a crossover exponent, to be determined [31, 32]. Thus, for any fixed $A \neq 0$, and $L_x \rightarrow \infty$ ($x \rightarrow 0$), three-dimensional features must dominate, while for $x \gg 1$ two-dimensional behavior (with finite-size corrections) will take over.

Furthermore, the data of Fig. 2 must collapse on the same curve, when plotted against x . This latter statement gives the operational procedure for determination of ϕ . By recalling that the horizontal axis variable in Fig. 2 can be written as $(L_x L_y)^{-1} = x^{2/\phi} A^{2/\phi-1}$, and that constant- A curves are further away from the vertical axis the larger A is, one sees that, in order for those curves to collapse one must have $\phi < 2$; consideration of the numerical values involved shows that, in fact, $\phi \lesssim 1$ is needed. The choice of $\phi = 0.95(3)$, with the corresponding results exhibited in Fig. 3, reflects the range of ϕ for which the collapse of all data for non-zero A (onto the left-hand side of the diagram) is visually deemed to be best. The fact that the $d = 2$ data are segregated towards the right is to be expected in this context, as they belong to a different side of the crossover ($x > 1$) where three-dimensional effects vanish.

The intersection of the scaling curve with the vertical axis provides an estimate of the three-dimensional scaling exponent. The result is $\tau(d = 3) = 1.27(1)$. An *ad hoc* parabolic fit against $1/L_x$, including only data for $A = 1$ and $L_x \leq 160$, gives $\tau(d = 3) = 1.28(1)$, where the largest contribution to the uncertainty comes from spread between extrapolations that either do or do not include small-lattice data ($L_x = 30, 40$). As we have seven lattice sizes available for $A = 1$, use of parabolic fits already gives us at most four degrees of freedom.

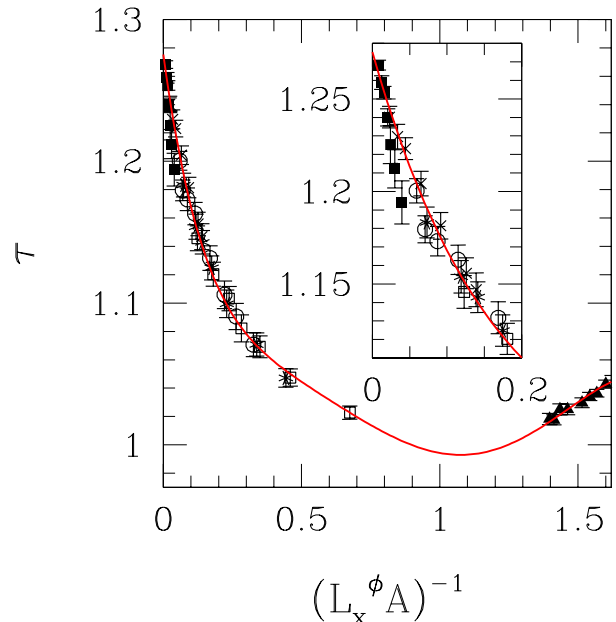


Figure 3: Effective exponent τ from fits of simulation data to Eq. (4), against crossover variable $x \equiv (L_x^{-1})^\phi/A$, with $\phi = 0.95$. Key to symbols is same as in caption to Fig. 2. Full line is a fourth-degree fitting curve with an exponential tail near $x = 0$. Inset shows details of main figure close to the vertical axis.

Given the limited range of data available, attempting to improve estimates by including higher-order corrections would therefore not seem justifiable. Since neither extrapolation procedure appears to be obviously superior to the other, our final quote encompasses both results: $\tau(d = 3) = 1.275(15)$.

In Ref. 7, $\tau(d = 3) = 1.13(2)$ is quoted for $L_x = 40$, while our corresponding result is $1.21(1)$. This difference arises mainly from distinct fitting procedures, in particular those authors’ apparent use of a fixed $\delta = 1$ for the cutoff. Indeed, by keeping $\delta = 1$, the best fit of our data is for $\tau(d = 3) = 1.12(4)$, though at the cost of increasing the χ^2 per degree of freedom by one order of magnitude compared with the variable- δ fitting scheme.

A similar parabolic fit of the two-dimensional data gathered on the right-hand corner of Fig. 3 (using $4000 \leq L_x \leq 16000$), gives $\tau(d = 2) = 1.06(1)$. This is broadly in accord with the result of Ref. 7, namely $\tau(d = 2) = 1.00(1)$ (using $500 \leq L_x \leq 5000$).

IV. ROUGHNESS DISTRIBUTIONS AND $1/f^\alpha$ NOISE

In this section, we consider only two-dimensional ($L_x = 1$) and fully three-dimensional ($L_x = L_y$) systems. We have collected data on interface roughness, in order to analyze them in the context of universal fluctuation

tuation distributions. An important reason for interest in universal distributions is that they have no adjustable parameters [20, 21, 22, 23]. The fact that a given property of a system behaves according to one of such distributions is then expected to indicate the universality class to which it belongs. For non-equilibrium problems such as is the case here, the task of connecting exponents (or features of distributions) to universality classes is far from accomplished (see e.g. the discussion in Ref. 23). Accordingly, our purpose here is simply to identify what universal distribution (if any) is followed by the scaled interface roughness for the current model.

In order to make contact with previous work on interface roughness at depinning transitions, we recall some basic ideas.

At the end of each avalanche, we measured the roughness \mathcal{R} of the instantaneous interface configuration at time t in the usual way, as the rms fluctuation of the interface height:

$$\mathcal{R}(t) = \left[(L_x L_y)^{-1} \sum_{i=1}^{L_x L_y} (h_i(t) - \bar{h}(t))^2 \right]^{1/2}, \quad (5)$$

where $\bar{h}(t)$ is the average interface height at t . As the avalanches progress, one gets a sampling of successive equilibrium configurations; the ensemble of such configurations yields a distribution of the relative frequency of occurrence of \mathcal{R} . In order to get clean distributions, we have seen that the number of events considered must be $\mathcal{O}(10^6)$, i.e. one order of magnitude larger than the samples used for the analysis of size distributions in Section III. We have used only steady-state data, i.e. after the stabilization of H_e of Eq. (2) against external field H . This way, our implicit assumption that successive interface configurations are stochastically independent gains plausibility. Similar ideas were invoked in Ref. 34 to justify a mapping of the steady state of a deposition-evaporation model onto a random-walk problem.

The roughness exponent ζ is related to the finite-size scaling of the first moment of the distribution [35]:

$$\langle \mathcal{R}_L \rangle \sim L^\zeta, \quad (6)$$

where the angular brackets stand for averages over the ensemble of successive interface configurations of an interface with transverse dimension L . We have estimated ζ from power-law fits to our data. For $d = 2$ (one-dimensional interface) using $400 \leq L_x \leq 1200$ we get $\zeta(2d) = 1.24(1)$, which compares well with the usually accepted $\zeta \simeq 1.25$ for the quenched Edwards-Wilkinson universality class [36, 37, 38, 39]. For $d = 3$ (two-dimensional interface) we used $30 \leq L_x = L_y \leq 80$ and two alternative sets of boundary conditions, namely mixed (MBC) i.e. free along x and periodic along y , as described in Section II, and periodic along both x and y (PBC). The results are, respectively, $\zeta(d = 3, \text{MBC}) = 0.87(1)$ and $\zeta(d = 3, \text{PBC}) = 0.71(1)$. While the latter value is not far from $\zeta \simeq 0.75$ for the corresponding

quenched Edwards-Wilkinson model [36, 39], the former seems difficult to relate to existing results.

At this point one might invoke universality ideas and claim that the difference between three-dimensional estimates must be a finite-size effect. Investigating this directly, e.g. by performing simulations for larger L , would be straightforward but time-consuming. However, as we shall see in what follows, this issue can be addressed more efficiently by returning to our main goal in this Section, i.e. by looking at the full distributions, rather than examining only selected moments (as is the case of the scaling for extraction of ζ). This is because mounting evidence indicates that, in general, width distributions decouple into the product of a single size-dependent scale and a universal (size-independent) scaling function [22, 23, 34, 40], that is

$$P(\mathcal{R}) = (1/\sigma) \Phi(\mathcal{R}/\sigma), \quad \sigma^2 = \langle (\mathcal{R} - \langle \mathcal{R} \rangle)^2 \rangle. \quad (7)$$

Therefore, if the functional form $\Phi(z)$ varies depending e.g. on whether mixed or periodic boundary conditions are used, one is on safer grounds to assume that this reflects differences in the respective universality class. In this context, it must be recalled that dependence of scaling quantities on boundary conditions is an often-encountered feature when dealing with fluctuation phenomena [22, 23]. One illustration of this, which is of great relevance here, is that one of the requirements for a class of universal (time) fluctuation distributions to hold is that they be periodic in time [22, 23, 34].

In our case, this feature is replaced by periodic boundary conditions *in space* (the same reasoning was used for the deposition-evaporation model of Ref. 34). Strictly speaking, this time-space correspondence is only true for the one-dimensional interfaces of the two-dimensional version of our model. However, the mixed boundary conditions (MBC) used in Sec. III suggest that an extension of our investigation to the three-dimensional case may not be unjustified. As regards fully periodic boundary conditions (PBC), even though it is not obvious that the analogy can be pushed that far, we decided to analyse the respective data for completeness.

We analysed the roughness distributions for $d = 2$ and for the fully three-dimensional case (i.e. aspect ratio $L_y/L_x = 1$), the latter both with MBC and PBC. As shown below, finite transverse dimensions are of negligible import as far as the scaling functions $\Phi(z)$ are concerned, thus giving further support to the assumption that Eq. (7) holds.

We have compared our results against the family of roughness distributions for periodic $1/f^\alpha$ noise, described in Ref. 23. The roughness of a time signal, and its connections via Fourier transform with the frequency spectrum (and thus with the respective α), are described at length in Section II of that reference. The idea of fitting spatial roughness data to the roughness of time signals (e.g. random-walks) is well-known in the study of interface fluctuations [35]. The new feature here is that we have at our disposal a family of distributions whose shape varies

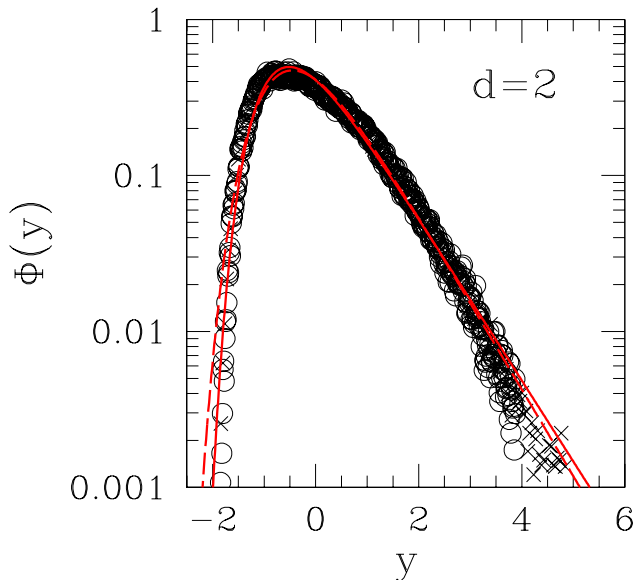


Figure 4: Scaled probability distributions $\Phi(y)$ in $d = 2$ for y defined in Eq. (8). Crosses: $L_x = 400$; circles: $L_x = 1000$. Lines are roughness distributions for $1/f^\alpha$ noise given in Ref. 23, with $\alpha = 1.15$ (full) and 1 (dashed).

smoothly against the single basic parameter α (but, apart from that, are strictly parameter-independent). We expect that the value of α which best fits our data should be connected to the underlying universality class of the avalanche model used here. We recall that ours is a phenomenological study, since at present very little is known regarding the (physical) causal relationships between fluctuation distributions and universality classes for out-of-equilibrium transitions [20, 21, 22, 23].

The quantity to be compared against a universal form is the distribution of the deviation from the average, scaled by the standard deviation (this is termed *scaling by the variance* in Ref. 23):

$$y \equiv \frac{\mathcal{R} - \langle \mathcal{R} \rangle}{\sigma}. \quad (8)$$

Our data are depicted respectively in Fig. 4 for $d = 2$, Fig. 5 for $d = 3$ with MBC, and Fig. 6 for $d = 3$ with PBC. In each figure, we have plotted data corresponding to only two values of L (“small” and “large”), in order to illustrate that the L -dependence of the scaled distribution is negligible, without cluttering the diagram with intermediate- L results. In all figures, the analytic curve corresponding to $\alpha = 1$ is shown as a dashed line, in order to ease comparison between different cases. In general, the scatter of simulational data at the low-roughness end of the distribution is much smaller than that at the high end, thus we might give more weight to the former region when judging the quality of fit. Using this criterion, one sees that the $d = 2$ data appear to be closer to the

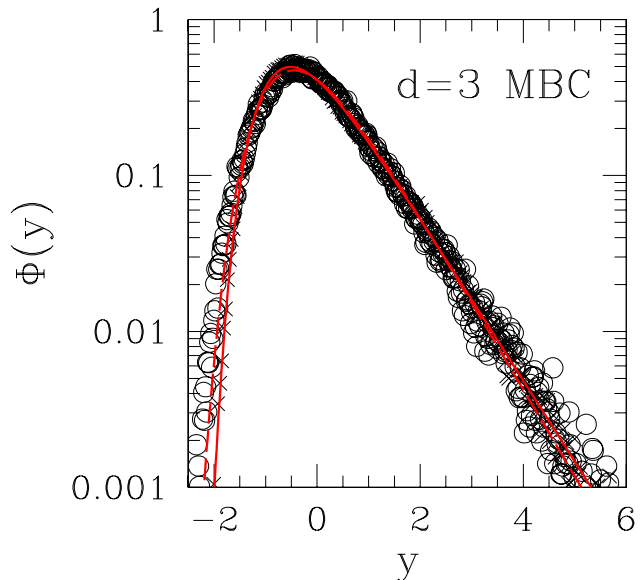


Figure 5: Scaled probability distributions $\Phi(y)$ in $d = 3$ with MBC, for y defined in Eq. (8). Crosses: $L = 30$; circles: $L = 80$. Lines are roughness distributions for $1/f^\alpha$ noise given in Ref. 23, with $\alpha = 1.15$ (full) and 1 (dashed).

$\alpha = 1.15$ curve than to that for $\alpha = 1$, while the situation is reversed in the $d = 3$ case with MBC. Furthermore, for $d = 3$ with PBC the best fit is undoubtedly for $\alpha < 1$. For this latter case, we also display a Gaussian distribution, which corresponds to $\alpha = 0.5$ [23]. We have tried to quantify the above remarks, by investigating the behavior of the χ^2 per degree of freedom ($\chi^2/\text{d.o.f.}$) for fits of our data to the analytical distributions, against varying α . We have included only data for which $\Phi(y) \geq 10^{-3}$, i.e. those displayed in Figs. 4, 5, and 6. Though, in principle, the distributions can be evaluated in closed form [23], we ran into serious numerical problems for $\alpha \lesssim 0.9$ in the region $y \lesssim -1$. Fortunately, as shown in Fig. 7, this does not matter much as long as the $d = 2$ and $d = 3$ (MBC) cases are concerned, because the respective $\chi^2/\text{d.o.f.}$ clearly exhibit minima located slightly above $\alpha = 1$. On the other hand, this means that for $d = 3$ with PBC we were not able to follow the trend shown in the Figure into the region $\alpha < 0.9$, where it is clear that a minimum of the corresponding $\chi^2/\text{d.o.f.}$ must be located. On the other hand, the Gaussian ($\alpha = 0.5$) distribution shown in Fig. 6 evidently overshoots the desired corrections, so one can be sure that the best fit will be in the interval $0.5 < \alpha < 0.9$.

V. DISCUSSION AND CONCLUSIONS

The data displayed in Section III show that, in the interface model introduced in Ref. 7, the power-law behav-

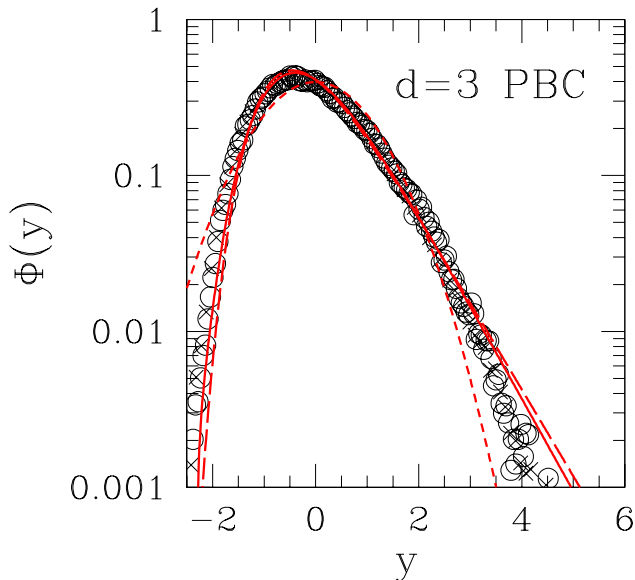


Figure 6: Scaled probability distributions $\Phi(y)$ in $d = 3$ with PBC for y defined in Eq. (8). Crosses: $L = 30$; circles: $L = 80$. Lines are roughness distributions for $1/f^\alpha$ noise given in Ref. 23, with $\alpha = 0.9$ (full), 1 (dashed) and 0.5 (short-dashed).

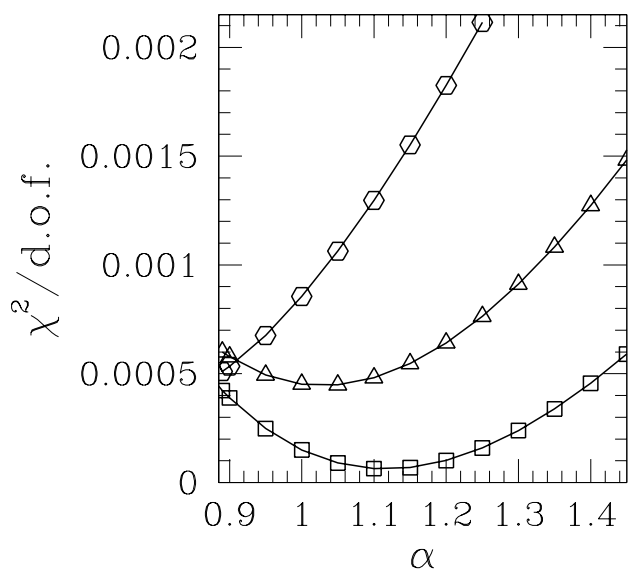


Figure 7: χ^2 per degree of freedom ($\chi^2/\text{d.o.f.}$) for fits of simulation data to analytical forms of $1/f^\alpha$ distributions, against α . Triangles: $d = 2$, $L_x = 400$; Squares: $d = 3$ MBC, $L = 40$; hexagons, $d = 3$ PBC, $L = 40$.

ior of avalanche statistics is characterized by an effective exponent, which varies continuously both with the interface's linear dimensions and aspect ratio. By means of a finite-size and crossover analysis, we have demonstrated that such continuous variation in fact reflects crossover towards three-dimensional behavior, for any non-zero aspect ratio.

The implications of this for the interpretation of experimental BN results in thin films must be worked out carefully. In Ref. 2, the value $\tau = 1.1$ is given for Fe films. The authors of Ref. 3 quote $\tau \simeq 1.33$ for Co films and conclude that their setup is a two-dimensional realization of the (single-interface) model of Ref. 9, for which $\tau = 4/3$ in $d = 2$ and $3/2$ in $d = 3$ [16, 41]. On the other hand, as seen above, the single-interface model considered here gives $\tau = 1.06(1)$ in $d = 2$ and $1.275(15)$ in $d = 3$. Thus one might interpret both sets of experimental results as reflecting a crossover towards three-dimensional behavior. As regards the specific features of the experimental investigations, one must ask: (i) which, if any, of the two models applies to the corresponding microscopic description, and (ii) how far along, quantitatively, is the dimensional crossover for the thin-film geometries used.

While the visual evidence displayed in Ref. 3 is convincing proof that a single-interface picture applies in that case, for a definite answer to (i) one must look at the differences between the models. As far as the power-law scaling of avalanche distributions is concerned, the model of Ref. 9 differs from the one considered here by the introduction of a non-local kernel due to dipolar interactions. The value $\tau = 4/3$ quoted in Ref. 3 relies on assuming that the form taken by this kernel in momentum space is $\sim q^\mu$, ($q = \text{wavevector}$) with $\mu = 1$ [41]. In $d = 3$ the same theory gives $\tau = 3/2$ for $\mu = 1$, and $\tau = 5/4$ for $\mu = 2$ [18]. Both values have been found to good approximation in experiments on fully three-dimensional systems (thus defining distinct universality classes), as recalled in the Introduction [18]. For the thin-film cases it is not clear, without a detailed analysis of the specific materials involved, whether the non-local kernel is of sufficient import to drive avalanche scaling towards the $d = 2$ behavior predicted for the model of Ref. 9.

Turning to question (ii), recall that the evolution of an interface along a $400 \times 320 \mu\text{m}^2$ area of a 25-nm film is shown in Ref. 3. Translating to the language of Section III, this would correspond to a transverse aspect ratio $A = 25\text{nm}/320\mu\text{m} \simeq 8 \times 10^{-5}$ (this in an upper bound, as the film's transverse dimensions are likely to be larger than the area shown). Though we do not think that the model results depicted in Fig. 2 are quantitatively accurate enough, one must keep in mind the possibility that the effective experimental behavior still is very close to the two-dimensional limit. Indeed, the simulational curve for $A = 5 \times 10^{-3}$ already shows a value of τ rather close to that for the two-dimensional case, along an extended portion of the Figure. The surest way to settle this matter would be by performing a series of experiments on films of the same composition and varying

thicknesses, in order to produce a full picture of the dimensional crossover. We hope experimentalists will be motivated by the present results.

As regards the search for universal roughness distributions in Section IV, for now we quote (from Figure 7 and the associated remarks) $\alpha \simeq 1.05$ ($d = 2$); $\alpha \simeq 1.15$ ($d = 3$, MBC) and $0.5 < \alpha < 0.9$ ($d = 3$, PBC). It thus appears that the boundary conditions do have significant influence in this context, a fact which remains to be more fully understood. Although the search for the physical origins of $1/f$ noise [42] is clearly of great interest, it appears that, at least for non-equilibrium phenomena as is the case here, we are still at a very preliminary stage. Again, it is hoped that the present results will motivate further research. Measurements of the roughness distributions for alternative models of BN [8, 9] would

be a natural extension of the this work, in order to check whether the above-quoted values of α are indeed universal within this subset of avalanche models.

Acknowledgments

The author thanks Belita Koiller and Monica Bahiana for many interesting discussions and suggestions. The research of S.L.A.d.Q. was partially supported by the Brazilian agencies CNPq (Grants No. 30.1692/81.5 and No. 47.4715/01.9), FAPERJ (Grant No. E26-152.195/2002), FUJB-UFRJ and Instituto do Milênio de Nanociências-CNPq.

-
- [1] H. Barkhausen, Phys. Z. **20**, 401 (1919).
 [2] E. Puppini, Phys. Rev. Lett. **84**, 5415 (2000).
 [3] D.-H. Kim, S.-B. Choe, and S.-C. Shin, Phys. Rev. Lett. **90**, 087203 (2003).
 [4] B. Alessandro, C. Beatrice, G. Bertotti, and A. Montorsi, J. Appl. Phys. **64**, 5355 (1988).
 [5] B. Alessandro, C. Beatrice, G. Bertotti, and A. Montorsi, J. Appl. Phys. **68**, 2901 (1990).
 [6] P. J. Cote and L. V. Meisel, Phys. Rev. Lett. **67**, 1334 (1991).
 [7] J. S. Urbach, R. C. Madison, and J. T. Markert, Phys. Rev. Lett. **75**, 276 (1995).
 [8] O. Perković, K. Dahmen, and J. P. Sethna, Phys. Rev. Lett. **75**, 4528 (1995).
 [9] P. Cizeau, S. Zapperi, G. Durin, and H. E. Stanley, Phys. Rev. Lett. **79**, 4669 (1997).
 [10] M. Bahiana, B. Koiller, S. L. A. de Queiroz, J. Denardin, and R. Sommer, Phys. Rev. E **59**, 3884 (1999).
 [11] B. Tadić, Physica A **270**, 125 (1999).
 [12] O. Perković, K. Dahmen, and J. P. Sethna, Phys. Rev. B **59**, 6106 (1999).
 [13] B. Tadić, Physica A **282**, 362 (2000).
 [14] B. Tadić and U. Nowak, Phys. Rev. E **61**, 4610 (2000).
 [15] M. C. Kuntz and J. P. Sethna, Phys. Rev. B **62**, 11 699 (2000).
 [16] S. Zapperi, P. Cizeau, G. Durin, and H. E. Stanley, Phys. Rev. B **58**, 6353 (1998).
 [17] G. Durin and S. Zapperi, J. Appl. Phys. **85**, 5196 (1999).
 [18] G. Durin and S. Zapperi, Phys. Rev. Lett. **84**, 4705 (2000).
 [19] S. L. A. de Queiroz and M. Bahiana, Phys. Rev. E **64**, 066127 (2001).
 [20] S. T. Bramwell, P. C. W. Holdsworth, and J.-F. Pinton, Nature (London) **396**, 552 (1998).
 [21] S. T. Bramwell, K. Christensen, J.-Y. Fortin, P. C. W. Holdsworth, H. J. Jensen, S. Lise, J. M. López, M. Nicodemi, J.-F. Pinton, and M. Sellitto, Phys. Rev. Lett. **84**, 3744 (2000).
 [22] T. Antal, M. Droz, G. Györgi, and Z. Rácz, Phys. Rev. Lett. **87**, 240601 (2001).
 [23] T. Antal, M. Droz, G. Györgi, and Z. Rácz, Phys. Rev. E **65**, 046140 (2002).
 [24] G. Bertotti, G. Durin, and A. Magni, J. Appl. Phys. **75**, 5490 (1994).
 [25] K. L. Babcock and R. M. Westervelt, Phys. Rev. Lett. **64**, 2168 (1990).
 [26] K. P. O'Brien and M. B. Weissman, Phys. Rev. E **50**, 3446 (1994).
 [27] D. Spasojević, S. Bukvić, S. Milošević, and H. E. Stanley, Phys. Rev. E **54**, 2531 (1996).
 [28] B. Tadić, Phys. Rev. Lett. **77**, 3843 (1996).
 [29] M. N. Barber, in *Phase Transitions and Critical Phenomena* (Academic, New York, 1983), edited by C. Domb and J. L. Lebowitz.
 [30] M. P. Nightingale, in *Finite Size Scaling and Numerical Simulations of Statistical Systems* (World Scientific, Singapore, 1990), edited by V. Privman.
 [31] R. B. Stinchcombe, in *Phase Transitions and Critical Phenomena*, vol. 7 (Academic, New York, 1983), edited by C. Domb and J. L. Lebowitz.
 [32] J. Cardy, *Scaling and Renormalization in Statistical Physics* (Cambridge University Press, Cambridge, 1996).
 [33] R. B. Stinchcombe, J. Phys. C **13**, 5565 (1980).
 [34] G. Foltin, K. Oerding, Z. Rácz, R. L. Workman, and R. K. P. Zia, Phys. Rev. E **50**, R639 (1994).
 [35] A.-L. Barabási and H. E. Stanley, *Fractal Concepts in Surface Growth* (Cambridge University Press, Cambridge, 1995).
 [36] H. Leschhorn, Physica A **195**, 324 (1993).
 [37] H. A. Makse and L. A. N. Amaral, Europhys. Lett. **31**, 379 (1995).
 [38] H. A. Makse, S. Buldyrev, H. Leschhorn, and H. E. Stanley, Europhys. Lett. **41**, 251 (1998).
 [39] A. Rosso, A. K. Hartmann, and W. Krauth, Phys. Rev. E **67**, 021602 (2003).
 [40] A. Rosso, W. Krauth, P. L. Doussal, J. Vannimenus, and K. J. Wiese, Phys. Rev. E **68**, 036128 (2003).
 [41] A. Vásquez and O. Sotolongo-Costa, Phys. Rev. Lett. **84**, 1316 (2000).
 [42] M. B. Weissman, Rev. Mod. Phys. **60**, 537 (1988).